

Anthony B. Davis*

Space & Remote Sensing Sciences Group, Los Alamos National Laboratory,
Los Alamos, New Mexico

Nikola P. Petrov

Department of Physics, University of Texas, Austin, Texas

Eugene E. Clothiaux

Department of Meteorology, Penn State University, University Park, Pennsylvania

1. Overview

The spatial and/or temporal variability of clouds is of paramount importance for at least two intensely researched sub-problems in global and regional climate modeling: cloud-radiation interaction where correlations can trigger 3D radiative transfer effects; and dynamical cloud modeling where the goal is to realistically reproduce the said correlations. We propose wavelets as a simple yet powerful way of quantifying cloud variability.

We introduce "semi-discrete" wavelet transforms which are discrete in scale, as in Mallat's (1989) efficient cascade technique known as "multi-resolution analysis," but they are continuous in position (Davis et al. 1999, and references therein). The number of coefficients and algorithmic complexity then grows only as $N \log N$, where N is the number of points (pixels) in the time-series (image). The redundancy of this representation at each scale has been exploited previously, using several different terminologies, in denoising and data compression applications but we see it as a safeguard when cumulating spatial statistics. Also, the wavelets are scaled so that the exponents of the statistical moments of the coefficients are the same as for structure functions at all orders, at least for nonstationary signals with stationary increments. By now, we have effectively relaxed the habitual constraints of orthogonality and normalization in wavelet theory (Daubechies 1992).

We apply 1D and 2D semi-discrete wavelet transforms to remote sensing data on cloud structure from two sources:

- an upward-looking mm cloud radar (MMCR) at DOE's climate observation site in Oklahoma supporting the Atmospheric Radiation Measurement (ARM) Program; and
- DOE's Multispectral Thermal Imager (MTI), a high-resolution instrument described in sufficient detail for our present purposes by Weber et al. (1999).

The scale-dependence of the variance of the wavelet coefficients always appears to be a better discriminator of transition from stationary to nonstationary behavior than conventional methods based on auto-correlation analysis, 2nd-order structure function (a.k.a. the semi-variogram), or spectral analysis. Consider the following examples

- Stationary behavior is found in uncorrelated instrumental noise at very small scales and after the large-scale decorrelation of cloudiness; here, wavelet coefficients decrease with increasing scale.
- Nonstationary behavior is found in the turbulence of horizontal structure in clouds as well as instrumental or physical smoothing in the data; here, wavelet coefficients increase with scale.

In all of these regimes, we have theoretical predictions for and/or empirical evidence of power-law relations for wavelet statistics with respect to scale, as expected in physical (finite scaling range) fractal phenomena. In particular, we have long-range correlations in cloud structure coming from the important nonstationary regime.

* *Corresponding author address:* Anthony B. Davis, LANL/NIS-2, P.O. Box 1663 (Mail Stop C-323), Los Alamos, NM 87545, USA; e-mail: adavis@lanl.gov.

Finally, we discuss artifacts we found in the data that are traceable either to instrumental noise or to post-processing liabilities.

2. Background on Wavelets and Scaling Laws

The wavelet transform of a signal $f(x)$ is essentially a convolution with a scaled version of an oscillating function ψ :

$$T_\psi[f](a, b) = \frac{1}{a} \int f(x) \psi\left(\frac{x-b}{a}\right) dx. \quad (1)$$

where x is real for a time-series and a 2D vector for an image. The arguments (a, b) are respectively the scale and position of the wavelet ψ . Figure 1 shows the Haar wavelet and its associated “scaling” function which simply gives an average over two elements. In the semi-discrete wavelet transform, we take $a = 2^j \times$ (pixel scale), where $j = 0, \dots, j_{max}$, while b covers all *possible* positions. That means all positions where the support of the wavelet is still inside the data field. The maximum scale of interest is determined by j_{max} which is set to $\lfloor \log_2 N \rfloor$ where N is the length of the times series, or to $\lfloor \log_2 \min\{N_x, N_y\} \rfloor$ for an image with $N = N_x \times N_y$ pixels. Note that the choice $\psi = \delta(x - (\text{pixel scale})) - \delta(x)$ in 1D brings us back to classic structure functions (Arneodo et al. 1995).

We will be seeking scaling relations for the wavelet coefficients in Eq. (1), i.e., a parametric representation of

$$\langle T_\psi[f](a, b)^2 \rangle_b \sim a^{2H}, \quad (2)$$

where $\langle \cdot \rangle_b$ means averaging over the argument b . The parameter H is a Hurst-like exponent that has the usual (Mandelbrot 1982) meaning when between 0 and 1 but can, in principle, be < 0 or > 1 depending on the choices of f and ψ . With the deliberately unconventional choice of normalization in (1), δ -correlated stationary (white) noise yields $H = -1/2$, “ $1/f$ ” noise yields $H = 0$, and smooth (everywhere differentiable) signals yield $H = 1$.

3. 1D Horizontal Transects of mm-Radar Reflectivity

We first analyze a 6-day long sequence of cloud mm-radar data collected at the ARM Southern Great Plains site, January 9–14, 1998. Vertical profiles of reflectivity $f(x) = Z(t, z)$, where $x = vt$, v being the appropriate advection velocity. A full suite of range bins with $\Delta z = 45$ m is captured every $\Delta t = 10$ s ($\Delta x = 50$ m at a nominal 5 m/s advection speed). The data are not very interesting to visualize. Indeed, during this long cloudy episode, there was always a low-level cloud occupying typically the first 20 levels, and not much else. We

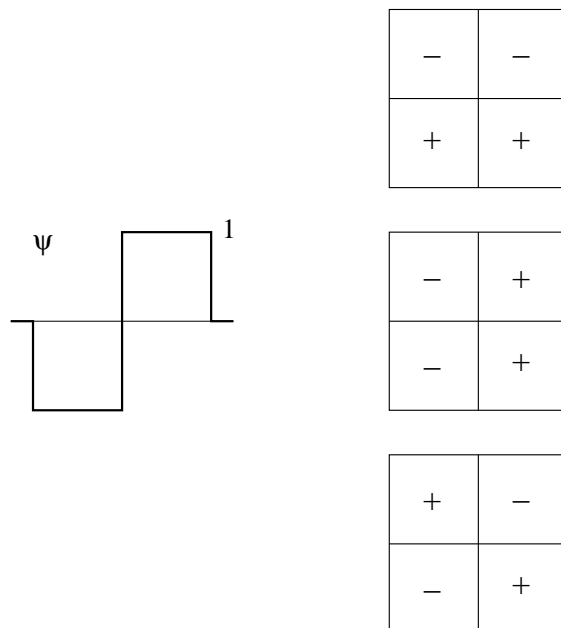


Figure 1: Haar wavelets in 1D (left) and in 2D (right).

performed 1D semi-discrete wavelet analyses for each level, using 5 short instances of linear interpolation to compensate for the data drop-out between days.

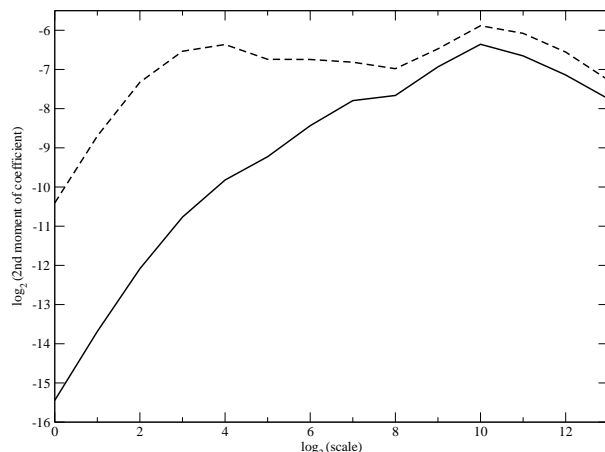


Figure 2: 1D semi-discrete wavelet spectrum analysis of horizontal layers of ARM cloud-radar data. Solid line – height 180 m, dashed line – 630 m.

Figure 2 shows a log-log plot of $\log_2 \langle T_\psi[f](a, b)^2 \rangle_b$ versus $\log_2 a$ for levels 180, m and 630 m respectively. The range of scales is huge, from 10 s to 10×2^{14} s, roughly 46 hours (corresponding to several hundred km).

We see that the lower layers exhibit three scaling regimes. As scale increases, we see a very smooth

regime, with H close to 1, followed by a regime with $H \approx 1/3$ which is characteristic of boundary-layer turbulence, and finally we see a stationary regime with $H < 0$. Keeping the mean wind at ≈ 5 m/s, transitions are respectively at ≈ 0.5 km and ≈ 50 km. The latter scale is probably exaggerated since the wind eventually meanders.

The small-scale transition from turbulence to smoothness is not observed in in-situ probings and it is in fact explained by the interpolation performed between 4 or more neighboring horizontal samples in the specific “best estimate” radar operation mode used here. As it turns out, this mode is designed for whole-column monitoring and compromises the sampling in the boundary layer. The interpolation remedy is safe in the sense of mean values but it corrupts the correlation structures. As an example, it would be very misleading to use these radar data at small scales to assess cloud model performance since in dynamical modeling too it is unfortunately necessary to introduce an artificial smoothing (in this case, it is to control small-scale numerical instabilities). *We recommend that either the temporal radar sampling be increased so that the interpolation becomes unnecessary or that the reflectivity profiles be archived at a resolution which is dynamically meaningful.*

In contrast, the large-scale transition is apparently real and probably related to the scale-breaks observed in reflected (Austin et al. 1999) and transmitted (Savigny et al. 2002) radiance fields at several tens of kilometers. The likely microphysical explanation for this scale-break is the cap imposed on liquid water path, hence its variability, in stratus layers by the onset of efficient drizzle production. This process is still poorly understood.

The higher layers exhibit just two scaling regimes: the same artificially smoothed regime as for the low levels, and a long essentially flat regime (for the wavelet coefficient). This corresponds to a “ $1/f$ ” spectrum and the change in scaling with height emphasizes the statistical anisotropy and heterogeneity of clouds.

4. 2D Correlations in MTI Cloud Data

We now turn to data from MTI, a high-resolution push-broom imaging spectro-radiometer with state-of-the-art calibration (especially in the thermal IR channels). In the visible/near-IR spectral region of interest here, the pixels have a mere 5 m footprint (better resolution is now commercially available, but only in panchromatic mode). We investigated a completely cloud-covered scene of opportunity (not illustrated) which is very smooth across the whole image. MTI’s focal plane has 3 sensor chip arrays (SCAs) that build up the complete swath. The most striking feature of the image is

indeed the two boundaries between SCAs. Since they are not systematically inter-calibrated, we analyze them separately.

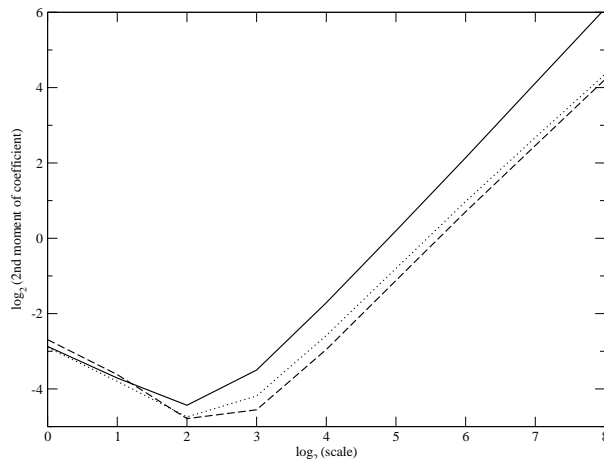


Figure 3: 2nd-order statistics for MTI cloud data: wavelet analysis of the x -variability for SCA 1 (solid line), SCA 2 (dotted line), SCA 3 (dashed line). Other wavelets in Fig. 1 give similar results.

Figure 3 shows wavelet energy spectra based on the 2D Haar transform in Fig. 1 for the 3 SCAs. Over these scales (5 m to 1.3 km), we expected a very smooth radiance field due to the horizontal transport of photons across many pixel scales via multiple scattering. This “radiative smoothing” has been quantified by Marshak et al. (1995) and others. We therefore anticipate H to be quite close to 1. This makes the scale-break in Fig. 3 around 2^2 pixels (20 m) rather intriguing. We find the expected H value at larger scales, and a *negative* H , characteristic of stationary noise, at smaller scales. The turn-around in wavelet energy occurs where signal equals noise. Note that, in this study, “signal” means the diminutive wavelet coefficients for a smooth field, not the overall photon counts, while “noise” (whatever its instrumental source may be) is amplified by taking differences of large quantities to compute the wavelet coefficient.

The origin of this detector noise is not fully understood. It is believed to be traceable to the extrapolation of radiometric calibration data gathered for relatively dark targets to the unusually bright (and indeed inadvertent) target in this cloudy image.

5. Summary

We have analyzed ground-based/active and satellite/passive remote sensing data on stratus cloud layers with semi-discrete wavelet transforms. For simplicity,

the piece-wise constant Haar wavelet was used in the 1D analysis of mm-radar transects, and its extension to 2D by tensor products for the satellite imagery. We confirmed the existence of well-known scaling laws and a lesser-known scale-break that ends the long-range correlations in cloud structure at a few tens of km.

Our most interesting finding is that scale-breaks in wavelet energy spectra can also be used to diagnose problems in the data, unsuspected artifacts. In this study alone, we found a deficit in variance (traceable to human intervention) and an excess of variance (traceable to an instrumental noise).

References

Arneodo, A., E. Bacry, and J.-F. Muzy, 1995: The thermodynamics of fractals revisited with wavelets, *Physica A*, **213**, 232-275.

Austin, P. H., M. Szsodorak, and G. Lewis, 1999: Spatial variability of satellite-retrieved optical depth and effective radius in marine stratocumulus clouds, in *Proceedings of 10th AMS Conference on Atmospheric Radiation*, pp. 237-240, June 28 - July 2, 1999, Madison (Wi), Am. Met. Soc., Boston (Ma).

Daubechies, I., 1992: *Ten Lectures on Wavelets*, CBMS-NSF Regional Conference Series in Applied Mathematics, 61. SIAM, Philadelphia (Pa).

Davis, A. B., A. Marshak, and E. E. Clothiaux, 1999: Anisotropic multi-resolution analysis in 2D, Application to long-range correlations in cloud mm-radar fields, in *S.P.I.E. Proceedings, vol. 3723: Wavelet Applications VI*, ed. H. H. Szu, pp. 194-207.

Mallat, S., 1989: A theory for multiresolution signal decomposition: The wavelet representation, *IEEE Trans. Pattern Anal. Mach. Intel.*, **11**, 674-693.

Mandelbrot, B. B., 1982: *The Fractal Geometry of Nature*, 460 pp., W. H. Freeman, San Fransisco (Ca).

Marshak, A., A. Davis, W. J. Wiscombe, and R. F. Cahalan, 1995: Radiative smoothing in fractal clouds, *J. Geophys. Res.*, **100**, 26,247-26,261.

Savigny, C. von, A. B. Davis, O. Funk, and K. Pfeilsticker, 2002: Time-series of zenith radiance and surface flux under cloudy skies: Radiative smoothing, optical thickness retrievals and large-scale stationarity, *Geophys. Res. Lett.*, in press.

Weber, P. G., B. C. Brock, A. J. Garrett, B. W. Smith, C. C. Borel, W. B. Clodius, S. C. Bender, R. Rex Kay,

and M. L. Decker, 1999: Multispectral Thermal Imager mission overview, in *S.P.I.E. Proceedings, vol. 3753: Imaging Spectrometry IV*, eds. M. R. Descour and S. S. Shen, pp. 340-346.